
Article:
Lio, W.H., Jones, B., Lu, Q. et al. (1 more author) (2015) Fundamental performance similarities between individual pitch control strategies for wind turbines. International Journal of Control. ISSN 1366-5820

https://doi.org/10.1080/00207179.2015.1078912

To appear in the *International Journal of Control*
Vol. 00, No. 00, Month 20XX, 1–22

Fundamental performance similarities between individual pitch control strategies for wind turbines

Wai Hou Lio[a] *, Bryn Ll. Jones[a], Qian Lu[b] and J.A. Rossiter[a]

[a] *Department of Automatic Control and Systems Engineering, The University of Sheffield, U.K.*;
[b] *Department of Mechanical Engineering Science, University of Surrey, U.K.*

(*Received xx xx 201x*)

The use of blade individual pitch control (IPC) offers a means of reducing the harmful turbine structural loads that arise from the uneven and unsteady forcing from the oncoming wind. In recent years two different and competing IPC techniques have emerged that are characterised by the specific loads that they are primarily designed to attenuate. In the first instance, methodologies such as single-blade control and Clarke Transform-based control have been developed to reduce the unsteady loads on the rotating blades, whilst tilt-yaw control and its many variants instead target load reductions in the non rotating turbine structures, such as the tower and main bearing. Given the seeming disparities between these controllers, the aim of this paper is to show the fundamental performance similarities that exist between them and hence unify research in this area. Specifically, we show that single-blade controllers are equivalent to a particular class of tilt-yaw controller, which itself is equivalent to Clarke Transform-based control. This means that three architecturally dissimilar IPC controllers exist that yield exactly the same performance in terms of load reductions on fixed and rotating turbine structures. We further demonstrate this outcome by presenting results obtained from high-fidelity closed-loop turbine simulations.

Keywords: Individual pitch control; single-blade control; Clarke-Transform; Coleman-Transform; tilt-yaw control.

1. Introduction

The ability possessed by most modern wind turbine generators to actively control the pitch of each blade offers the potential to reduce the unsteady loads that arise form a number of sources, such as wind-shear, tower shadow, yaw misalignment and turbulence within the atmospheric boundary layer (Barlas & van Kuik, 2010). Such loads are a known source of the structural fatigue damage that can reduce the operational lifetime of a turbine, ultimately increasing the cost of wind energy to the end user. As a consequence, a growing body of research has emerged in recent years, seeking to establish the best way of designing individual pitch control (IPC) systems. Typically, and for reasons of simplicity of implementation favoured by the industry, IPCs are designed separately from a collective pitch control (CPC) system, whose role is to regulate the rotor speed in above-rated wind conditions by collectively adjusting the pitch angle of each blade by the same amount (Muljadi & Butterfield, 2001; Pao & Johnson, 2009). The IPC provides an additional pitch angle demand signal, typically in response to measurements of the flap-wise blade root bending moments, in order to attenuate the effects of unsteady spatio-temporal rotor loads.

Of the many IPC strategies that have been published in recent years, most can be grouped into two distinct classes, characterised by the specific turbine loads they are primarily designed to attenuate. The first and most populous branch of IPC targets load reductions on the non-rotating

*Corresponding author. Email: w.h.lio@sheffield.ac.uk

turbine structures, such as the tower, nacelle and main bearing. A coordinate transformation is employed to refer sensing and actuation signals in the rotating frame of reference to a non-rotating reference frame. The most commonly employed transformation in this respect is the Coleman Transform. As noted by Lu, Bowyer, and Jones (2014), this transformation emerged from the area of helicopter rotor control (Coleman & Feingold, 1957), and is widely employed in the fields of power conversion and electrical machines under the guise of the direct-quadrature-zero (dq0) transform (Vas, 1992). Use of the Coleman Transform to address the IPC problem was adopted by Bossanyi (2003) and van Engelen and van der Hooft (2005) in order to project blade loads onto the non-rotating and orthogonal turbine tilt and yaw axes. Subsequent IPC design then attenuates the tilt and yaw referred loads, with such designs sometimes referred to as 'tilt-yaw' controllers. These produce tilt and yaw referred pitch demand signals which are projected back to the rotating frame of reference via the inverse Coleman Transform. The attractive feature of the Coleman Transform is that it transforms an otherwise time periodic system into one that is time-invariant by projecting the system inputs and outputs in the rotational frame of reference onto stationary tilt and yaw axes. If the turbine dynamics are linear, or can be approximated as such, then conventional tools of linear and time-invariant (LTI) control system design can further be applied to design controllers to attenuate the unsteady loads upon the non-rotating turbine structures. This is the main reason why the majority of IPC studies have employed the Coleman Transform (Bossanyi, 2003, 2005; Bossanyi & Wright, 2009; Engels, Subhani, Zafar, & Savenije, 2014; Geyler & Caselitz, 2008; Lackner & van Kuik, 2010; Lu et al., 2014; Plumley, Leithead, Jamieson, Bossanyi, & Graham, 2014; Selvam, Kanev, van Wingerden, van Engelen, & Verhaegen, 2009; Stol, Moll, Bir, & Namik, 2009; van Engelen, 2006; van Engelen & van der Hooft, 2005).

The second branch of IPC targets load reductions upon the rotating turbine structures, primarily the blades. Single-blade control (W. Leithead, Neilson, & Dominguez, 2009; W. E. Leithead, Neilson, Dominguez, & Dutka, 2009), later termed individual blade control (Han & Leithead, 2014), equips each blade with its own controller that actuates in response to local blade load measurements. The overall IPC controller is thus formed from three identical single-input-single-output (SISO) controllers acting independently from one another. Although conceptually simple, there is redundancy in the sense that three separate SISO controllers are not necessary to design an IPC controller. Recently, (Zhang, Chen, & Cheng, 2013) showed it was possible to use just two identical SISO controllers, pre and post-compensated by the Clarke Transform (Vas, 1992) and its inverse to yield good blade-load reductions. This form of blade load IPC was termed proportional-resonant control by these authors. It is interesting to note that the Clarke Transform, also known as the $\alpha\beta\gamma$ Transform, is conceptually similar to the Coleman Transform in the sense that both transforms perform projections onto a set of orthogonal axes. However, whereas the Coleman Transform performs a projection onto a set of axes that are rotating with respect to the turbine blades, the Clarke Transform performs a projection onto a set of axes that are stationary with respect to the blades. One immediate implication of this, as noted by Zhang et al. (2013) is that the Clarke Transform-based IPC does not require a measurement of the rotor azimuth angle, unlike IPC based upon the Coleman Transform. The same benefit also holds for single-blade control.

Given this range of IPC techniques, it is natural to attempt to understand under what conditions these different controllers yield similar performance, in terms of load reductions. However, this is not as straightforward as it may seem. The fashion in which load reductions about the tilt and yaw axes correspond to reductions in blade loads is somewhat complicated by virtue of the frequency shifting effects of the Coleman Transform (Lu et al., 2014). Wind turbine loads predominantly exist at the harmonics of the blade rotational frequency (Barlas & van Kuik, 2010). For three-bladed turbines, the blade loads are concentrated at integer multiples of the once per revolution (1p) blade frequency, resulting in non-rotating loads at adjacent harmonics to the nearest 3p frequency (Zhang et al., 2013). For example, 1p blade loads map to static (0p) loads in the tilt and yaw frame of reference, whilst 3p non-rotating structural loads are split into 2p and 4p blade loads. It is this frequency shifting of loads that makes IPC comparisons difficult, and understanding this problem forms the essence of this paper.

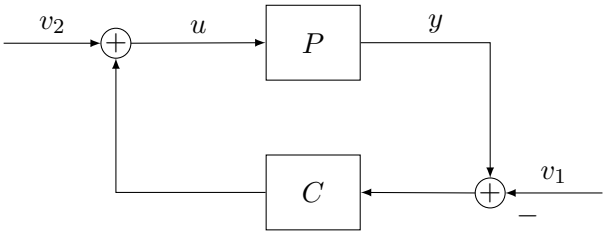

Figure 1. Standard feedback interconnection between plant P and controller C. The signals u and y denote the plant input and measured output, respectively, whilst v_1 and v_2 represent exogenous disturbances.

The remainder of this paper is structured as follows. Section 2 defines the three different IPCs under comparison. These are a Coleman Transform-based controller, a Clarke Transform-based controller, and a single-blade controller. In Section 3, the equivalence between these IPCs is established. Specifically, this paper shows; (i) that a single-blade controller is equivalent to a Coleman Transform-based controller with a particular structure; (ii) that this Coleman Transform-based controller is equivalent to a Clarke Transform-based controller; and (iii) that all three IPCs yield identical performance, as quantified by the robust stability margin. In Section 4, this equivalence is demonstrated by performing separate closed-loop simulations upon a high-fidelity wind turbine model, followed by a discussion of the results, with conclusions in Section 5.

Preliminaries

Let R and C denote the real and complex fields, respectively, $j := \sqrt{-1}$ and let $s \in \mathrm{C}$ denote a complex variable. All signals in this paper belong to $\mathcal{L}_2[0,\infty)$; the time-domain Lebesgue space of all signals of bounded energy supported on $[0,\infty)$, with norm $\|\cdot\|_2$. Let $\mathcal{R}$ denote the space of proper real-rational transfer function matrices and let $P^*(s) := P(-s)^T$ denote the adjoint of $P(s) \in \mathcal{R}$. $\mathcal{RH}_\infty$ is the space of proper real-rational transfer function matrices of stable, LTI continuous-time systems with norm $\|\cdot\|_\infty$. The maximum singular value of a matrix is denoted $\bar{\sigma}(\cdot)$. The standard feedback interconnection $[P,C]$ of plant $P \in \mathcal{R}$ and controller $C \in \mathcal{R}$ is shown in Figure 1, from which the following closed-loop system is defined:

$$\begin{bmatrix} y \\ u \end{bmatrix} = \underbrace{\begin{bmatrix} P \\ I \end{bmatrix} (I - CP)^{-1} \begin{bmatrix} -C & I \end{bmatrix}}_{H(P,C)} \begin{bmatrix} v_1 \\ v_2 \end{bmatrix}, \tag{1}$$

where $H(P,C) \in \mathcal{R}$ provided $[P,C]$ is well posed, and I is an identity matrix of compatible dimension. The robust stability margin $b(P,C) \in \mathrm{R}$ of $[P,C]$ is defined as follows (Vinnicombe, 2001):

$$b(P,C) := \begin{cases} \|H(P,C)\|_\infty^{-1} & \text{if } H(P,C) \in \mathcal{RH}_\infty \\ 0 & \text{otherwise.} \end{cases} \tag{2}$$

2. Individual Pitch Control

A typical wind turbine control systems architecture for above-rated conditions is shown in Figure 2. The CPC regulates the rotor speed $\omega(t)$ by adjusting the collective pitch angle $\bar{\theta}(t)$. To isolate the action of IPC from that of CPC, it is convenient to define the pitch angles and blade moments as

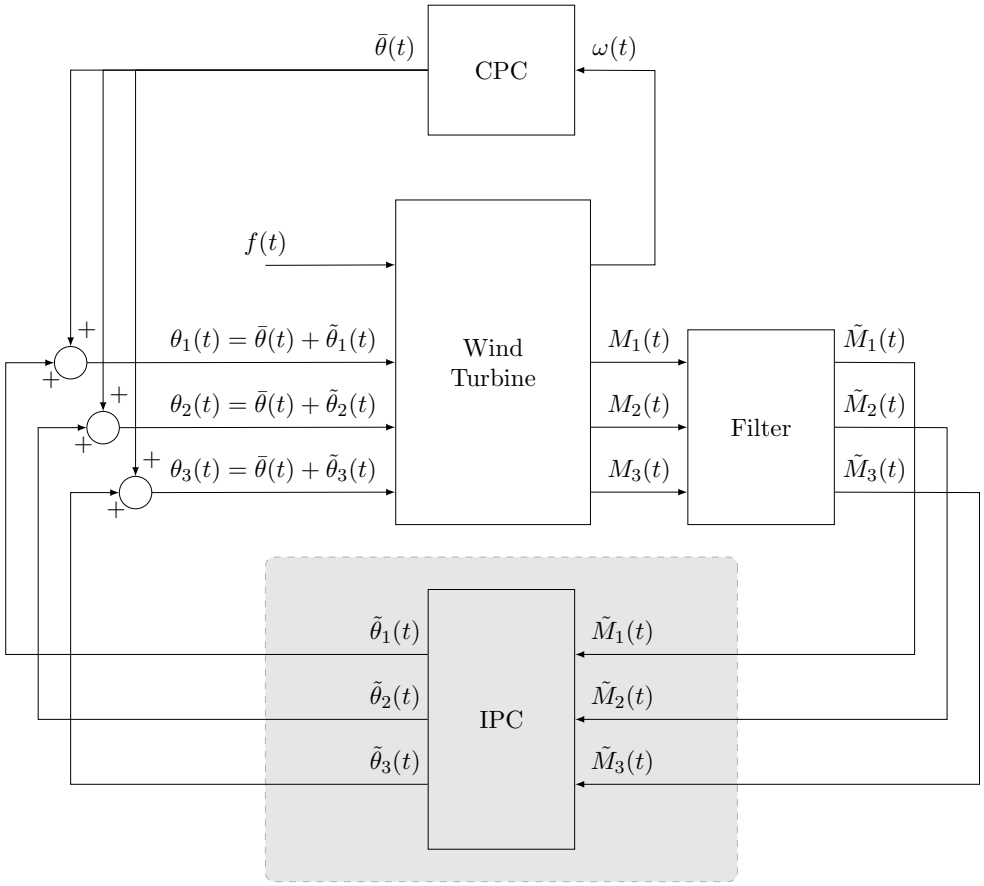

Figure 2. System architecture of a wind turbine, combining collective pitch control (CPC) and individual pitch control (IPC). The CPC regulates rotor speed while the IPC (shaded) attenuates perturbations in the flap-wise root bending moments on each blade. Additional inputs to the turbine such as wind loading and generator torque are accounted for in the term $f(t)$.

follows:

$$\begin{bmatrix}\theta_1(t)\\ \theta_2(t)\\ \theta_3(t)\end{bmatrix} := \begin{bmatrix}\bar{\theta}(t)+\tilde{\theta}_1(t)\\ \bar{\theta}(t)+\tilde{\theta}_2(t)\\ \bar{\theta}(t)+\tilde{\theta}_3(t)\end{bmatrix}, \qquad \begin{bmatrix}M_1(t)\\ M_2(t)\\ M_3(t)\end{bmatrix} := \begin{bmatrix}\bar{M}(t)+\tilde{M}_1(t)\\ \bar{M}(t)+\tilde{M}_2(t)\\ \bar{M}(t)+\tilde{M}_3(t)\end{bmatrix}, \tag{3}$$

where $\tilde{\theta}_{1,2,3}(t)$ represent the perturbations in blade pitch angle demand from the collective pitch signal, whilst $\tilde{M}_{1,2,3}(t)$ are the perturbations in flap-wise blade bending moments, obtained by filtering out the mean moment $\bar{M}(t)$ from the measurements $M_{1,2,3}(t)$. This filtering is important in order to help decouple the IPC from the CPC. For each blade, the relationship between perturbation input $\tilde{\theta}_i$ and output $\tilde{M}_i$, for $i \in \{1,2,3\}$ can be modelled by a transfer function $G \in \mathcal{R}$, obtaining by linearising the turbine dynamics around the rated rotor speed ω_0. A typical blade transfer function, as used by Lu et al. (2014) for example, is as follows:

$$G(s) := G_{\mathrm{a}}(s)G_{\mathrm{b}}(s)G_{\mathrm{bp}}(s), \tag{4a}$$

where $G_{\mathrm{a}}, G_{\mathrm{b}} \in \mathcal{R}$ describe the dynamics of the pitch actuator and the blade, respectively, whilst $G_{\mathrm{bp}} \in \mathcal{R}$ is a band-pass filter that is included in order to remove the low and high frequency components of the flap-wise blade root bending moment signals, obtained from strain-gauge

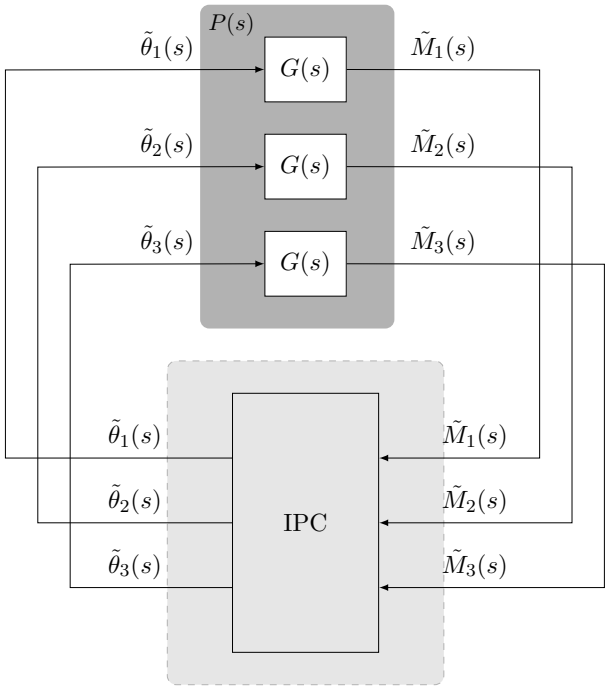

Figure 3. Basic system architecture for IPC analysis and design.

sensors. Basic models for each of these transfer functions are as follows:

$$G_{\mathrm{a}}(s) := \frac{1}{1+\tau s}, \tag{4b}$$

$$G_{\mathrm{b}}(s) := \frac{dM_{\mathrm{flap}}}{d\theta}\frac{(2\pi f_{\mathrm{b}})^2}{s^2 + D_{\mathrm{b}}2\pi f_{\mathrm{b}}s + (2\pi f_{\mathrm{b}})^2}, \tag{4c}$$

$$G_{\mathrm{bp}}(s) := \frac{2\pi f_{\mathrm{h}}s}{s^2 + 2\pi(f_{\mathrm{h}}+f_{\mathrm{l}})s + 4\pi^2 f_{\mathrm{h}}f_{\mathrm{l}}}, \tag{4d}$$

where $\tau \in \mathrm{R}$ is the pitch actuator time constant, $\frac{dM_{\mathrm{flap}}}{d\theta} \in \mathrm{R}$ represents the change in blade flap-wise bending moment with respect to pitch angle, $f_{\mathrm{b}} \in \mathrm{R}$ is the natural frequency of the blade's first flap-wise mode and $D_{\mathrm{b}} \in \mathrm{R}$ is its aerodynamic damping ratio, while $f_{\mathrm{h}}, f_{\mathrm{l}} \in \mathrm{R}$ are the high and low corner frequencies, respectively, of the bandpass filter. The basic individual pitch control problem is shown in Figure 3 and is based upon the following three-blade model:

$$\begin{bmatrix}\tilde{M}_1(s)\\ \tilde{M}_2(s)\\ \tilde{M}_3(s)\end{bmatrix} = \underbrace{\begin{bmatrix}G(s) & 0 & 0\\ 0 & G(s) & 0\\ 0 & 0 & G(s)\end{bmatrix}}_{P(s)} \begin{bmatrix}\tilde{\theta}_1(s)\\ \tilde{\theta}_2(s)\\ \tilde{\theta}_3(s)\end{bmatrix}. \tag{5}$$

In the interests of simplicity, the influence of the fixed turbine structural dynamics have not been included, but if required, these could be represented as additive disturbances on the bending moment channels. The next section introduces the three different IPCs employed in this study. These are shown in Figure 4, beginning first with the Coleman Transform-based controller.

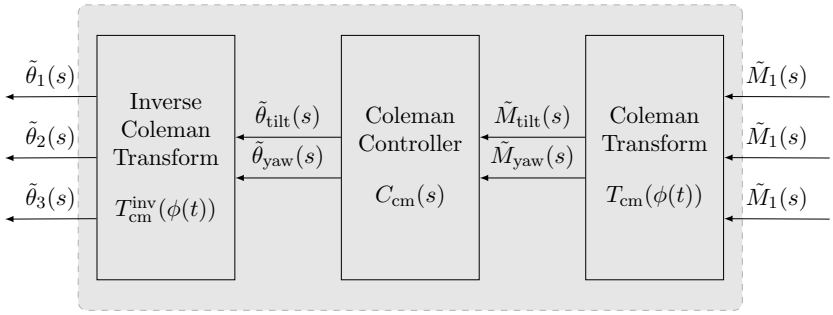

(a) Coleman Transform-based controller.

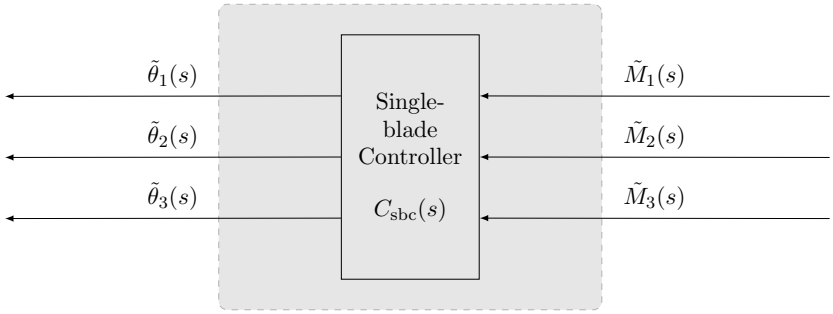

(b) Single-blade controller.

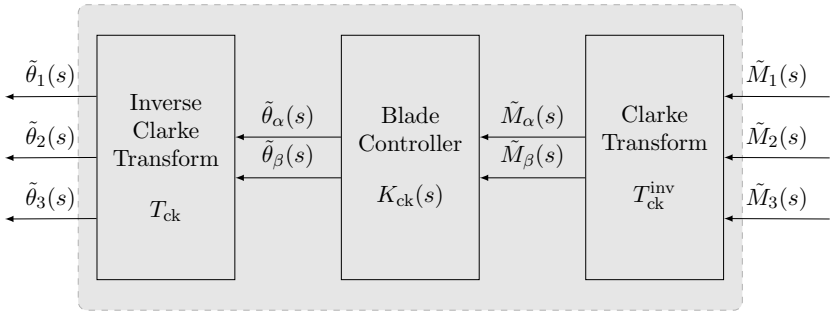

(c) Clarke Transform-based controller.

Figure 4. Three different IPC architectures.

2.1 *Coleman Transform-based control*

The Coleman Transform-based controller is shown in Figure 4(a). As discussed in Section 1, many IPC studies have employed this form of IPC in order to attenuate unsteady loads upon the fixed turbine structure. The Coleman Transform $T_{\rm cm}\left(\phi(t)\right)$ is a time varying matrix that projects the rotational blade loads onto the stationary and orthogonal tilt and yaw axes of the turbine, according to the blade azimuth angle $\phi(t)$. For a three-bladed turbine in which $\phi(t)$ is defined as the angle of the first blade from the horizontal yaw axis, the Coleman Transform is defined as follows:

$$\begin{bmatrix}\tilde{M}_{\rm tilt}(t)\\ \tilde{M}_{\rm yaw}(t)\end{bmatrix} := \underbrace{\frac{2}{3}\begin{bmatrix}\sin\phi(t) & \sin\left(\phi(t)+\frac{2\pi}{3}\right) & \sin\left(\phi(t)+\frac{4\pi}{3}\right)\\ \cos\phi(t) & \cos\left(\phi(t)+\frac{2\pi}{3}\right) & \cos\left(\phi(t)+\frac{4\pi}{3}\right)\end{bmatrix}}_{T_{\rm cm}(\phi(t))}\begin{bmatrix}\tilde{M}_1(t)\\ \tilde{M}_2(t)\\ \tilde{M}_3(t)\end{bmatrix}. \tag{6a}$$

The tilt and yaw referred flap-wise blade root bending moments, $\tilde{M}_{\rm tilt}$ and $\tilde{M}_{\rm yaw}$ are mapped via the Coleman controller $C_{\rm cm} \in \mathcal{R}^{2\times 2}$ to tilt and yaw referred pitch signals $\tilde{\theta}_{\rm tilt}$ and $\tilde{\theta}_{\rm yaw}$, that in turn are

projected back into the blade referred pitch signals via the inverse Coleman Transform, $T_{\rm cm}^{\rm inv}(\phi(t))$ accordingly:

$$\begin{bmatrix}\tilde{\theta}_1(t)\\ \tilde{\theta}_2(t)\\ \tilde{\theta}_3(t)\end{bmatrix} := \underbrace{\begin{bmatrix} \sin\phi(t) & \cos\phi(t) \\ \sin\left(\phi(t)+\frac{2\pi}{3}\right) & \cos\left(\phi(t)+\frac{2\pi}{3}\right) \\ \sin\left(\phi(t)+\frac{4\pi}{3}\right) & \cos\left(\phi(t)+\frac{4\pi}{3}\right)\end{bmatrix}}_{T_{\rm cm}^{\rm inv}(\phi(t))} \begin{bmatrix}\tilde{\theta}_{\rm tilt}(t)\\ \tilde{\theta}_{\rm yaw}(t)\end{bmatrix}. \tag{6b}$$

A basic Coleman controller consists of a diagonal transfer function matrix with equal proportional-integral terms along the diagonal. Such a controller implicitly assumes that the dynamics of the tilt and yaw axes are decoupled. However, this was shown not to be the case in Lu et al. (2014). By modelling the dynamics of the Coleman Transform and its inverse, Lu et al. (2014) showed how these operators modify the basic plant dynamics (5) to yield the Coleman-transformed plant $P_{\rm cm} \in \mathcal{R}^{2\times 2}$:

$$\begin{bmatrix}\tilde{M}_{\rm tilt}(s)\\ \tilde{M}_{\rm yaw}(s)\end{bmatrix} = \underbrace{\begin{bmatrix} \frac{G(s+j\omega_0)+G(s-j\omega_0)}{2} & j\frac{G(s+j\omega_0)-G(s-j\omega_0)}{2} \\ -j\frac{G(s+j\omega_0)-G(s-j\omega_0)}{2} & \frac{G(s+j\omega_0)+G(s-j\omega_0)}{2}\end{bmatrix}}_{P_{\rm cm}(s,\omega_0)} \begin{bmatrix}\tilde{\theta}_{\rm tilt}(s)\\ \tilde{\theta}_{\rm yaw}(s)\end{bmatrix}, \tag{7}$$

where $\omega_0 \in \mathrm{R}$ is the constant rated rotor speed, and from which the coupled nature of the tilt and yaw loops is evident. Lu et al. (2014) subsequently designed a $\mathcal{H}_\infty$ loop-shaping controller, based on $P_{\rm cm}$, that outperformed a comparative diagonal controller. By weighting $P_{\rm cm}$ with a diagonal precompensator containing integral terms and inverse notch filters at the 3p frequency, the resulting multivariable controller not only attenuated the 0p and 3p fixed structure loads, but also simultaneously attenuated the 1p, 2p and 4p blade loads.

2.2 *Single-blade control*

The simplest form of IPC is single-blade control, in which each blade is equipped with its own controller $K \in \mathcal{R}$ that acts in response to the local blade load measurements. Single-blade control is depicted in Figure 4(b), wherein the controller $C_{\rm sbc} \in \mathcal{R}^{3\times 3}$ has the following decoupled structure:

$$\begin{bmatrix}\tilde{\theta}_1(s)\\ \tilde{\theta}_2(s)\\ \tilde{\theta}_3(s)\end{bmatrix} = \underbrace{\begin{bmatrix} K(s) & 0 & 0 \\ 0 & K(s) & 0 \\ 0 & 0 & K(s)\end{bmatrix}}_{C_{\rm sbc}(K(s))} \begin{bmatrix}\tilde{M}_1(s)\\ \tilde{M}_2(s)\\ \tilde{M}_3(s)\end{bmatrix} \tag{8}$$

The blade controller K is typically designed to attenuate the blade loads at 1p, 2p and 4p frequencies. The benefits of this approach over those employing the Coleman Transform are that it can be realised as three, separate SISO controllers and also does not require a measurement of the rotor azimuth angle.

2.3 *Clarke Transform-based control*

Another IPC technique, based on blade load reductions, was recently introduced by Zhang et al. (2013) and employed the Clarke Transform to project the blade loads onto a pair of orthogonal axes that are stationary with respect to the turbine blades. Such a controller is shown in Fig-

ure 4(c), and consists of a diagonal blade controller $K_{\rm ck} \in \mathcal{R}^{2\times 2}$ pre and post-compensated by the Clarke Transform $T_{\rm ck} \in \mathrm{R}^{3\times 2}$ and its inverse $T_{\rm ck}^{\rm inv} \in \mathrm{R}^{2\times 3}$, as follows:

$$\begin{bmatrix}\tilde{\theta}_1(s)\\ \tilde{\theta}_2(s)\\ \tilde{\theta}_3(s)\end{bmatrix} := \underbrace{T_{\rm ck}^{\rm inv} K_{\rm ck}(K(s)) T_{\rm ck}}_{C_{\rm ck}(K(s))} \begin{bmatrix}\tilde{M}_1(t)\\ \tilde{M}_2(t)\\ \tilde{M}_3(t)\end{bmatrix}, \tag{9a}$$

where:

$$T_{\rm ck}^{\rm inv} = \sqrt{\frac{2}{3}}\begin{bmatrix}1 & 0\\ -\frac{1}{2} & \frac{\sqrt{3}}{2}\\ -\frac{1}{2} & -\frac{\sqrt{3}}{2}\end{bmatrix}, \qquad K_{\rm ck}(K(s)) = \begin{bmatrix}K(s) & 0\\ 0 & K(s)\end{bmatrix}, \qquad T_{\rm ck} = \sqrt{\frac{2}{3}}\begin{bmatrix}1 & -\frac{1}{2} & -\frac{1}{2}\\ 0 & \frac{\sqrt{3}}{2} & -\frac{\sqrt{3}}{2}\end{bmatrix}. \tag{9b}$$

As with the single-blade controller, the blade controllers K in the Clarke controller $C_{\rm ck}$ are designed to minimise the loads at 1p, 2p and 4p frequencies, but do so upon the orthogonally projected blade load signals $\tilde{M}_\alpha(t)$ and $\tilde{M}_\beta(t)$, as opposed to $\tilde{M}_{1,2,3}(t)$. Similarly to the single-blade controller, the Clarke controller does not require a measurement of the blade azimuth angle and the control design amounts to the design of a single SISO blade controller. However, the Clarke controller achieves its load reductions using only two SISO controllers, suggesting a degree of redundancy exists in the single-blade controller (8).

3. Equivalence of single-blade, Coleman and Clarke Transform-based controllers

In this Section, for a given blade controller K, the equivalence between the blade load IPCs, $C_{\rm sbc}(K)$ (8), $C_{\rm ck}(K)$ (9) and a particular type of Coleman Transform-based controller $C_{\rm cm}$ is established. This leads to the main result of the paper (Theorem 1) that proves that the performance of all three controllers is identical.

3.1 *Equivalence between single-blade and Coleman Transform-based control*

The equivalence between single-blade control and Coleman Transform-based control is first established. This amounts to ascertaining the form that a single-blade controller takes when referred to tilt and yaw coordinates via the Coleman Transforms. The following lemma establishes this equivalence.

Lemma 1: *Assuming a constant rotor speed $\omega(t) = \omega_0$, Coleman Transforms* (6) *and a given blade controller K, a single-blade controller $C_{\rm sbc}(K)$* (8) *is equivalent to the Coleman Transform-based controller $C_{\rm cm}(K, \omega_0)$, where:*

$$C_{\rm cm}(K(s), \omega_0) := \begin{bmatrix}\frac{K(s+j\omega_0)+K(s-j\omega_0)}{2} & j\frac{K(s+j\omega_0)-K(s-j\omega_0)}{2}\\ -j\frac{K(s+j\omega_0)-K(s-j\omega_0)}{2} & \frac{K(s+j\omega_0)+K(s-j\omega_0)}{2}\end{bmatrix} \tag{10}$$

Proof. The proof makes use of the following identities:

$$\mathcal{L}\left[u(t)\cos\phi(t)\right] = \mathcal{L}\left[u(t)\frac{e^{j\omega_0 t}+e^{-j\omega_0 t}}{2}\right] = \frac{1}{2}\left(U(s-j\omega_0)+U(s+j\omega_0)\right), \tag{11a}$$

$$\mathcal{L}\left[u(t)\sin\phi(t)\right] = \mathcal{L}\left[u(t)\frac{j\left(e^{-j\omega_0 t}-e^{j\omega_0 t}\right)}{2}\right] = \frac{j}{2}\left(U(s+j\omega_0)-U(s-j\omega_0)\right), \tag{11b}$$

where $u(t)$ is an arbitrary input signal, $U(s)$ is its Laplace transform and $\phi(t)=\omega_0 t$ is assumed. Inserting (11) into (6) yields:

$$\begin{bmatrix}\tilde{M}_1(s)\\ \tilde{M}_2(s)\\ \tilde{M}_3(s)\end{bmatrix} = C_-^T\begin{bmatrix}\tilde{M}_{\text{tilt}}(s-j\omega_0)\\ \tilde{M}_{\text{yaw}}(s-j\omega_0)\end{bmatrix} + C_+^T\begin{bmatrix}\tilde{M}_{\text{tilt}}(s+j\omega_0)\\ \tilde{M}_{\text{yaw}}(s+j\omega_0)\end{bmatrix}, \tag{12a}$$

$$\begin{bmatrix}\tilde{\theta}_{\text{tilt}}(s)\\ \tilde{\theta}_{\text{yaw}}(s)\end{bmatrix} = \frac{2}{3}C_-\begin{bmatrix}\tilde{\theta}_1(s-j\omega_0)\\ \tilde{\theta}_2(s-j\omega_0)\\ \tilde{\theta}_3(s-j\omega_0)\end{bmatrix} + \frac{2}{3}C_+\begin{bmatrix}\tilde{\theta}_1(s+j\omega_0)\\ \tilde{\theta}_2(s+j\omega_0)\\ \tilde{\theta}_3(s+j\omega_0)\end{bmatrix}, \tag{12b}$$

where C_- and C_+ are defined as:

$$C_- := \frac{1}{2}\begin{bmatrix}1 & -j\\ j & 1\end{bmatrix}\begin{bmatrix}\sin(0) & \sin(\frac{2\pi}{3}) & \sin(\frac{4\pi}{3})\\ \cos(0) & \cos(\frac{2\pi}{3}) & \cos(\frac{4\pi}{3})\end{bmatrix}, \quad C_+ := \frac{1}{2}\begin{bmatrix}1 & j\\ -j & 1\end{bmatrix}\begin{bmatrix}\sin(0) & \sin(\frac{2\pi}{3}) & \sin(\frac{4\pi}{3})\\ \cos(0) & \cos(\frac{2\pi}{3}) & \cos(\frac{4\pi}{3})\end{bmatrix}. \tag{12c}$$

Substituting (12) into (8) yields (10). □

It is interesting to note that the Coleman controller (10) possesses the same structure as the Coleman transformed plant (7), in much the same way as the single-blade controller (8) shares the diagonal structure of the turbine blade model (5). In view of this, the controller (10) will henceforth be termed a structured Coleman Transform-based controller.

3.2 *Equivalence between structured Coleman Transform and Clarke Transform-based controllers*

The projection from single-blade to tilt-yaw control via the Coleman Transforms yielded the structured Coleman Transform-based controller (10). However, the projection of (10) back to the rotating frame of reference does not yield the single-blade controller (8). Instead, it yields a Clarke Transform-based controller (9), according to the following lemma.

Lemma 2: *Assuming a constant rotor speed $\omega(t)=\omega_0$, Coleman Transforms* (6) *and a given blade controller K, the structured Coleman Transform-based controller $C_{\text{cm}}(K,\omega_0)$* (10) *is equivalent to $C_{\text{ck}}(K)$* (9)*.*

Proof. Referring to Figure 4(a) and using the relationships (10) and (12), the derivation is as

follows:

$$\begin{aligned}
\begin{bmatrix}\tilde{\theta}_1(s)\\ \tilde{\theta}_2(s)\\ \tilde{\theta}_3(s)\end{bmatrix} &= C_-^T \begin{bmatrix}\tilde{\theta}_{\text{tilt}}(s-j\omega_0)\\ \tilde{\theta}_{\text{yaw}}(s-j\omega_0)\end{bmatrix} + C_+^T \begin{bmatrix}\tilde{\theta}_{\text{tilt}}(s+j\omega_0)\\ \tilde{\theta}_{\text{yaw}}(s+j\omega_0)\end{bmatrix},\\
&= C_-^T C_{\text{cm}}(s-j\omega_0) \begin{bmatrix}\tilde{M}_{\text{tilt}}(s-j\omega_0)\\ \tilde{M}_{\text{yaw}}(s-j\omega_0)\end{bmatrix} + C_+^T C_{\text{cm}}(s+j\omega_0) \begin{bmatrix}\tilde{M}_{\text{tilt}}(s+j\omega_0)\\ \tilde{M}_{\text{yaw}}(s+j\omega_0)\end{bmatrix},\\
&= \frac{2}{3}\left[C_-^T C_{\text{cm}}(s-j\omega_0)\left(C_- \begin{bmatrix}\tilde{M}_1(s-2j\omega_0)\\ \tilde{M}_2(s-2j\omega_0)\\ \tilde{M}_3(s-2j\omega_0)\end{bmatrix} + C_+ \begin{bmatrix}\tilde{M}_1(s)\\ \tilde{M}_2(s)\\ \tilde{M}_3(s)\end{bmatrix}\right) + \dots\right.\\
&\qquad \left. \dots + C_+^T C_{\text{cm}}(s+j\omega_0)\left(C_- \begin{bmatrix}\tilde{M}_1(s)\\ \tilde{M}_2(s)\\ \tilde{M}_3(s)\end{bmatrix} + C_+ \begin{bmatrix}\tilde{M}_1(s+2j\omega_0)\\ \tilde{M}_2(s+2j\omega_0)\\ \tilde{M}_3(s+2j\omega_0)\end{bmatrix}\right)\right],\\
&= \begin{bmatrix}\frac{2}{3}K(s) & -\frac{1}{3}K(s) & -\frac{1}{3}K(s)\\ -\frac{1}{3}K(s) & \frac{2}{3}K(s) & -\frac{1}{3}K(s)\\ -\frac{1}{3}K(s) & -\frac{1}{3}K(s) & \frac{2}{3}K(s)\end{bmatrix} \begin{bmatrix}\tilde{M}_1(s)\\ \tilde{M}_2(s)\\ \tilde{M}_3(s)\end{bmatrix},\\
&= C_{\text{ck}}(s) \begin{bmatrix}\tilde{M}_1(s)\\ \tilde{M}_2(s)\\ \tilde{M}_3(s)\end{bmatrix}.
\end{aligned}$$

□

At this point the separate relationships have been established between a structured Coleman Transform-based controller, and single-blade and Clarke Transform-based controllers, respectively. The next section establishes the extent to which these three types of IPC behave in a similar fashion, as quantified by the robust stability margin (2).

3.3 *Performance equivalence of C_{sbc}, C_{ck} and C_{cm}*

The main result of this paper is as follows:

Theorem 1: *For a given blade model G (4) assume the turbine model $P(G)$ (5), and for a given fixed rotor speed ω_0 and blade controller K, form the IPC controllers $C_{\text{sbc}}(K)$, $C_{\text{ck}}(K)$ and $C_{\text{cm}}(K,\omega_0)$ according to (8), (9) and (10), respectively. Then the robust stability margin for each IPC is the same. Specifically,*

$$b(GK,1) = b(PC_{\text{sbc}},I) = b(PC_{\text{ck}},I) = b(PC_{\text{cm}},I). \tag{13}$$

Proof. See Appendix A. □

This suggests that the three different IPC strategies studied in this paper behave in exactly the same fashion. This is indeed the case, as shown in the following section.

4. Numerical Results and Discussion

The objective of this section is to demonstrate the performance equivalence of the various IPCs by performing closed-loop simulations of each controller upon upon a high-fidelity wind turbine model. The turbine model employed for this purpose is the NREL 5MW baseline turbine (J. Jonkman,

Table 1. Turbine simulation parameters

Rating	5 MW
Rotor Orientation	Upwind
Rotor diameter	126 m
Hub height	90 m
Rated rotor speed	12.1 rpm ($\approx$ 0.2 Hz)

Table 2. Model parameters of $G(s)$

Parameters	Values	Units
τ	0.11	s
$\frac{dM_{\text{flap}}}{d\theta}$	1.50 $\times 10^6$	Nm deg^{-1}
f_{b}	0.70	Hz
D_{b}	47.70	
f_{h}	0.80	Hz
f_{l}	0.014	Hz

Butterfield, Musial, & Scott, 2009) with the key parameters listed in Table 1, and the simulations carried out on FAST (J. Jonkman & Buhl Jr, 2005). Note that this model is of much greater complexity than the model employed for IPC design (5), and with the exception of the yaw axis, all degrees-of-freedom were enabled, including flap-wise and edge-wise blade modes, in addition to tower and shaft dynamics. The closed-loop simulations were performed under a representative and turbulent wind field that was generated from TurbSim (B. J. Jonkman, 2009) and the full-field three-dimensional wind velocity data was characterised by a mean wind speed of 18 ms^{-1}, chosen since this value is near the centre of the range of wind speeds covering above-rated wind conditions, turbulence intensity of 14% and vertical shear power law exponent of 0.2. The simulations were performed at an above-rated mean wind speed of 18 ms^{-1} and were run for sufficient duration to obtain convergence in the load spectra of the various key rotating and non-rotating turbine components.

4.1 *Controller design*

The three IPCs studied in this paper, (8), (9) and (10) are each a function of the underlying blade controller K. In turn, the design of K is based upon the basic blade model G (4a), whose parameters are listed in Table 2, and which has the following transfer function:

$$G(s) = \frac{1.45 \times 10^8 s}{0.11s^5 + 2.02s^4 + 13.84s^3 + 52.25s^2 + 101.50s + 8.54}. \tag{14}$$

Based on this model, a $\mathcal{H}_\infty$ loop-shaping controller K was designed to attenuate blade loads specifically at the 1p, 2p and 4p frequencies (0.2 Hz, 0.4 Hz and 0.8 Hz respectively), as shown in Figure 5. The resulting controller is presented in Appendix B and yielded a robust stability margin $b(GK, 1) = 0.39$. Based on this controller, the IPCs (8), (9) and (10) were generated and tested in simulation, as shown next.

4.2 *IPC simulation results upon the NREL 5MW turbine.*

Closed-loop simulations were performed upon each IPC and results were obtained to compare the load reductions on both the blades as well as the fixed turbine structures. Figure 6(a) shows the power spectrum of the flap-wise blade bending moment upon a particular blade, whilst Figures 6(b) and 6(c) display the power spectra of the main bearing tilt and yaw bending moments. With respect to the blade loads (Figure 6(a)), the performance of the separate IPCs are almost identical and display clear load reductions around the 1p and 2p frequencies, as compared to the uncontrolled turbine. In addition, there are further slight reductions at the 4p frequency. This is to be expected given the designed loop-shape of GK, as shown in Figure 5. The load reductions at these

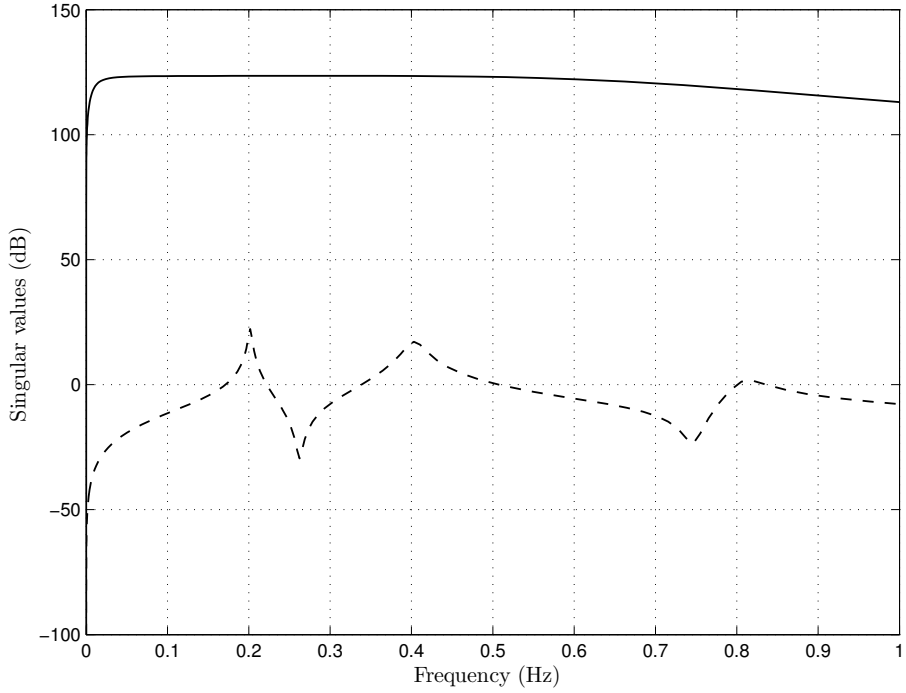

Figure 5. Maximum singular value plots of the wind turbine model $\bar{\sigma}(G(s))$ (–) and compensated system $\bar{\sigma}(GK(s))$ (- -).

frequencies translate to reductions at 0p and 3p frequencies in the fixed turbine structures as is evident from Figures 6(b) and 6(c), where again, the performance of the separate IPCs are almost indistinguishable. Given the performance similarities, it is no surprise that the pitch activity from each IPC is almost identical, as shown in Figure 6(d).

There is an important detail to note at this point. Close inspection of the results displayed in Figure 6 reveals that although the performance of the three IPCs is almost identical, there nevertheless exist some small differences, particularly between the structured Coleman Transform-based controller and its counterparts. This is at odds with Theorem 1, which suggests that there should be no performance difference. The reasons for this are explained next.

4.3 *Discussion*

The slight discrepancies in IPC performance arise from an assumption of the turbine operating with a constant rotor speed. In practice, this is difficult to achieve owing to the limitations of the CPC, in addition to the coupling between CPC and IPC through the tower dynamics (Selvam et al., 2009). This challenge to maintaining fixed rotor speed can clearly be seen in Figure 6(d) for the case without IPC, where changes in rotor speed are causing the CPC to continuously adjust the blade pitch angle. The structured Coleman Transform-based controller (10) is designed based upon an assumption of fixed rotor speed, and so perturbations to the rotor speed will inevitably result in deterioration in controller performance, although this is likely to be very small. To demonstrate this is indeed the case, the simulations of Section 4.2 were repeated, but in the absence of tower dynamics. This cancels the fore-aft motion of the turbine and thus eliminates a major source of disturbance to the collective-pitch loop that regulates the rotor speed. With this in mind, Figure 7 displays the load spectra and pitch activity, from which it is clear that the performance of the various IPCs is indistinguishable.

Given the essentially identical performance from the various IPCs, the question of 'which is best' is not straightforward to answer, and may rest with issues of implementation and load design priorities. For instance, the implementation of single-blade control is arguably the simplest; essentially

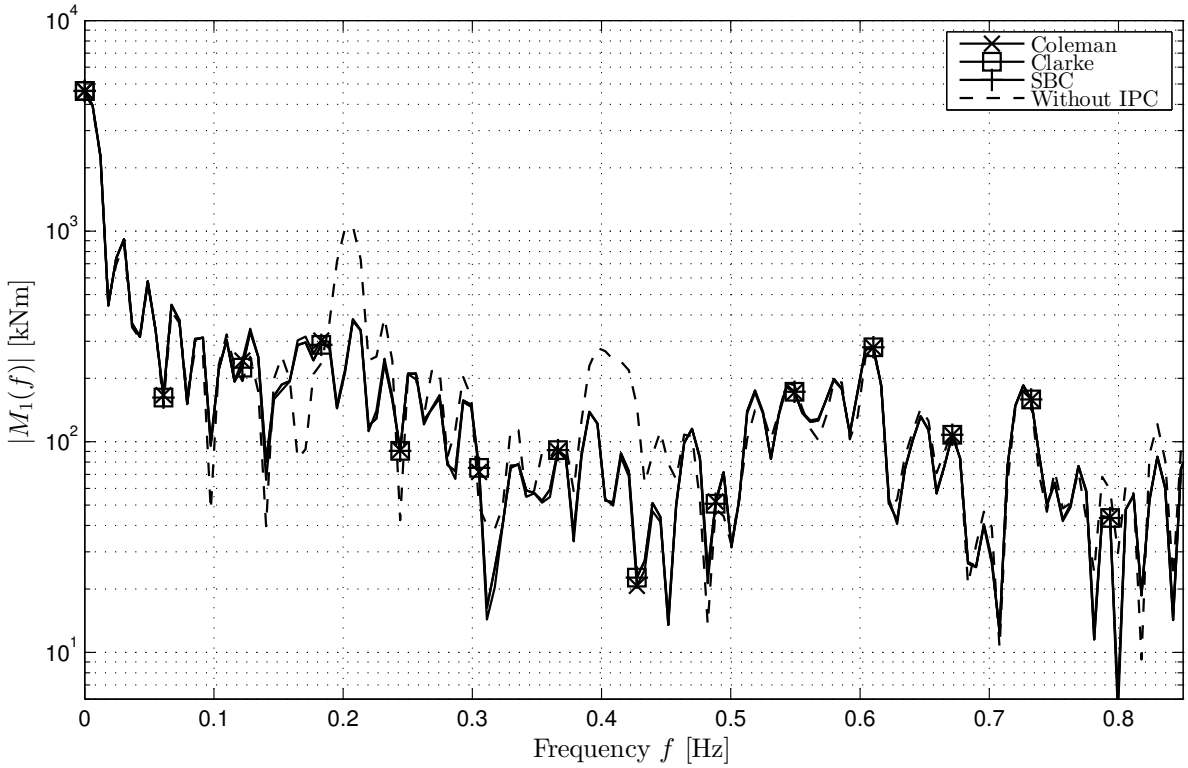

(a) Power spectrum of the flap-wise blade bending moment of blade 1. The same spectra are obtained for the other blades.

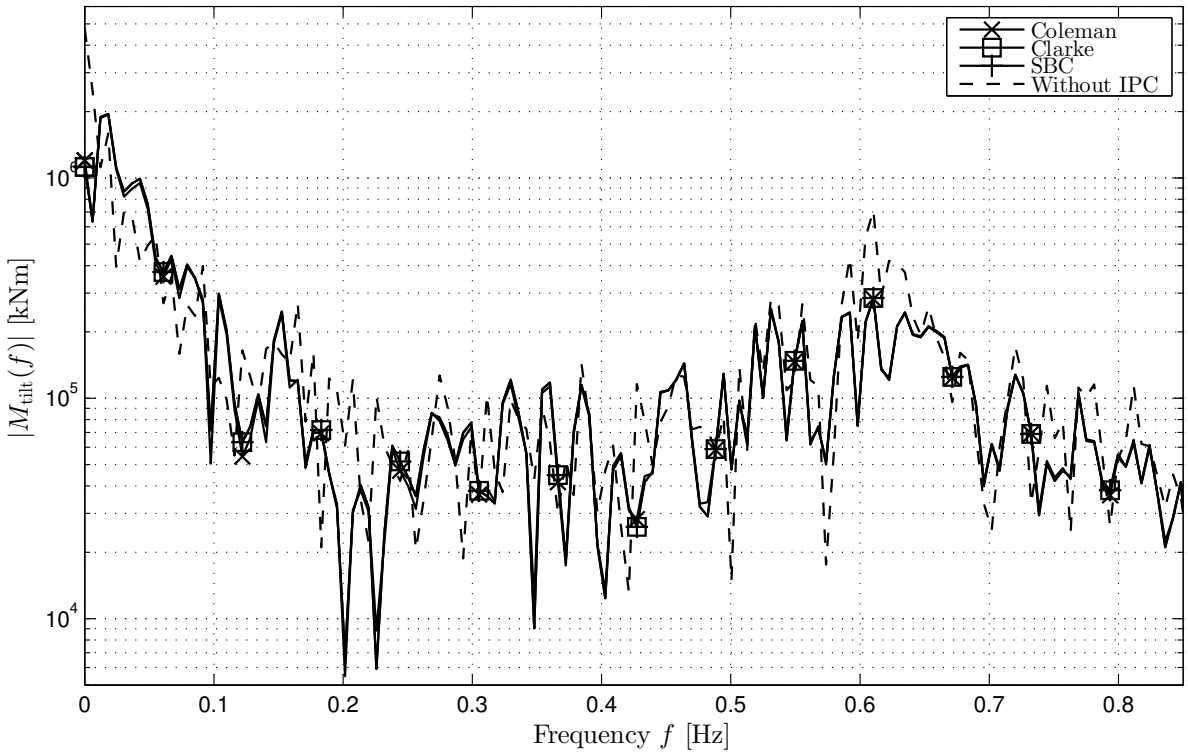

(b) Power spectrum of the main bearing tilt bending moment.

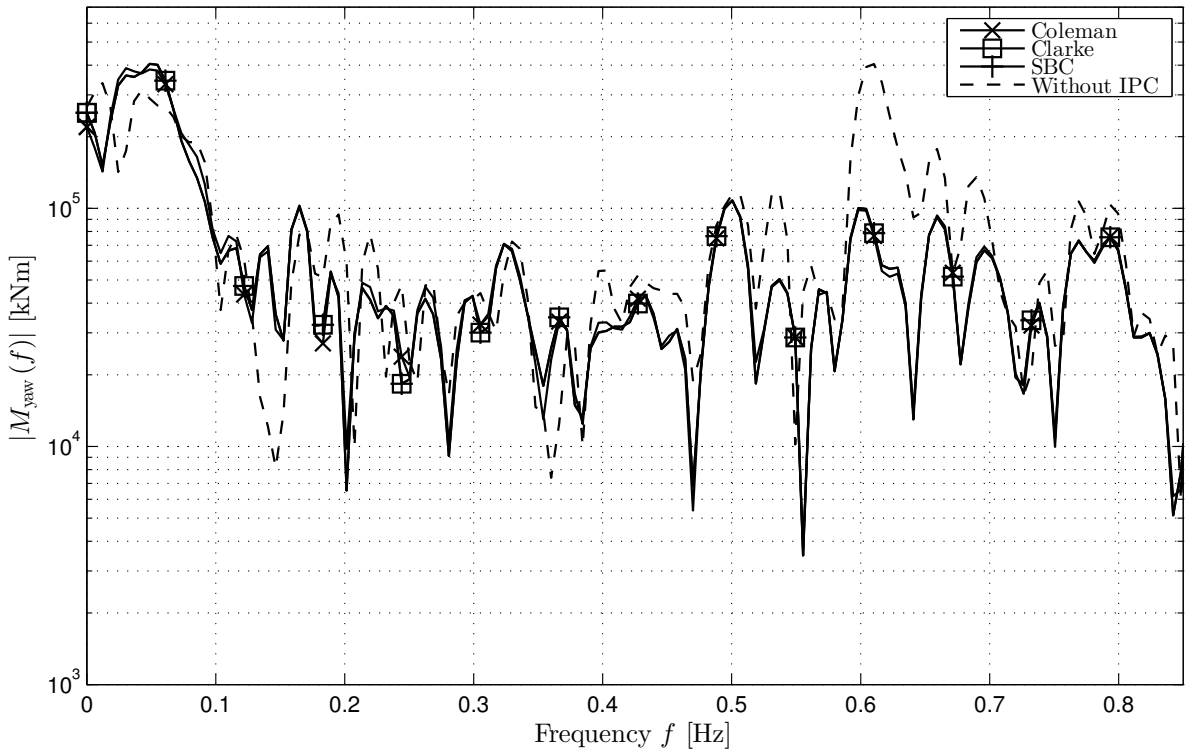

(c) Power spectrum of the main bearing yaw bending moment. Similar results are observed as in Fig 6(b)

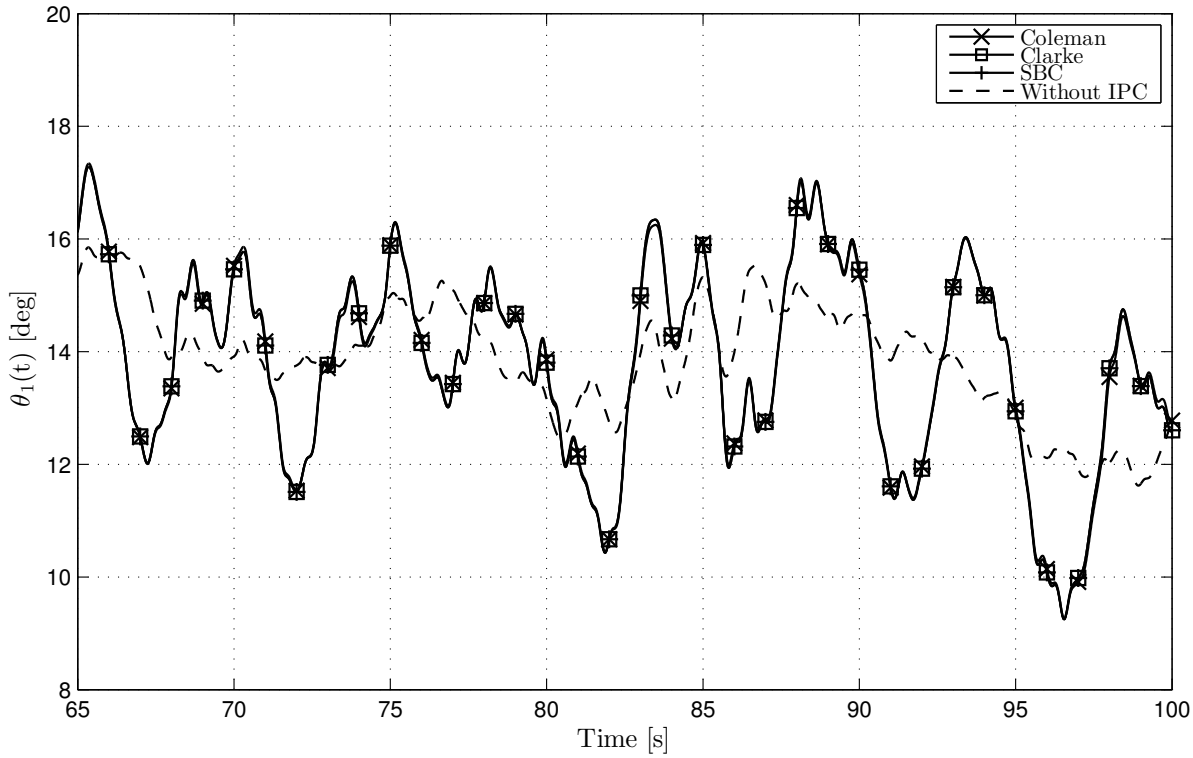

(d) Time history of the blade-pitch angle of blade 1. Similar plots are obtained for the other blades.

Figure 6. Simulation results upon the NREL 5MW turbine, showing the performance similarities between the various IPCs studied in this paper.

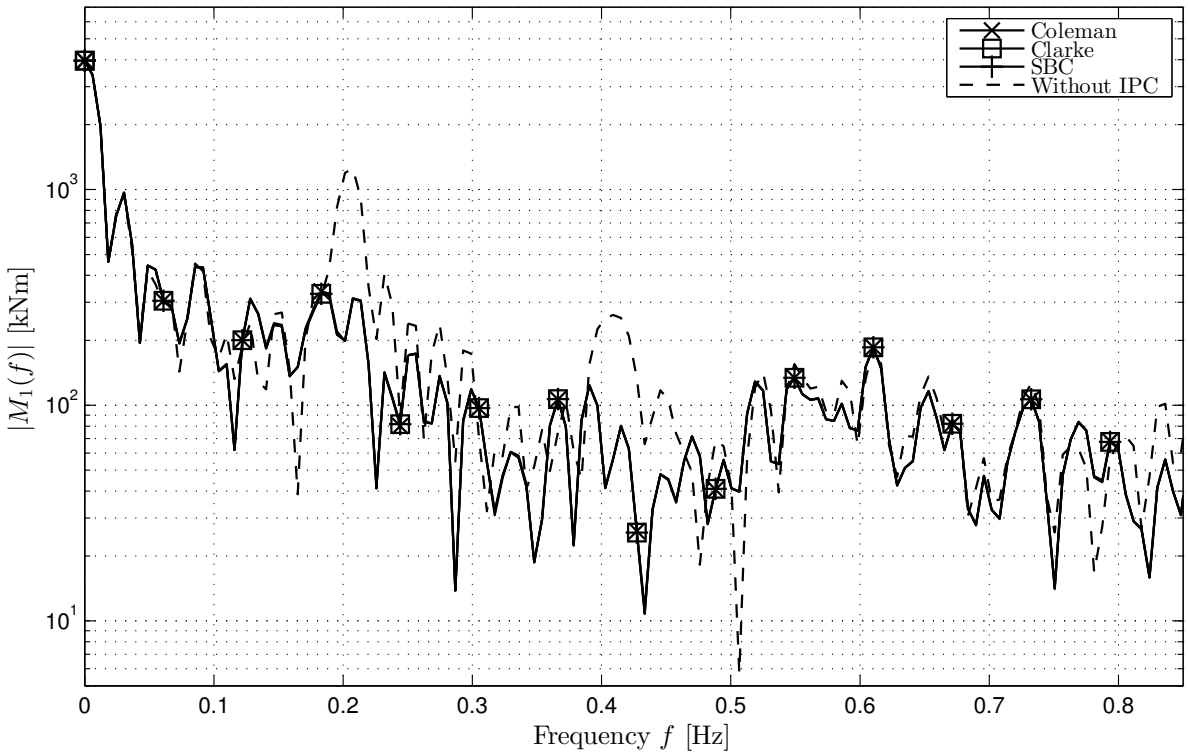

(a) Power spectrum of the flap-wise blade root bending moment of blade 1, with fixed rotor speed. The same power spectrum is observed for all blades.

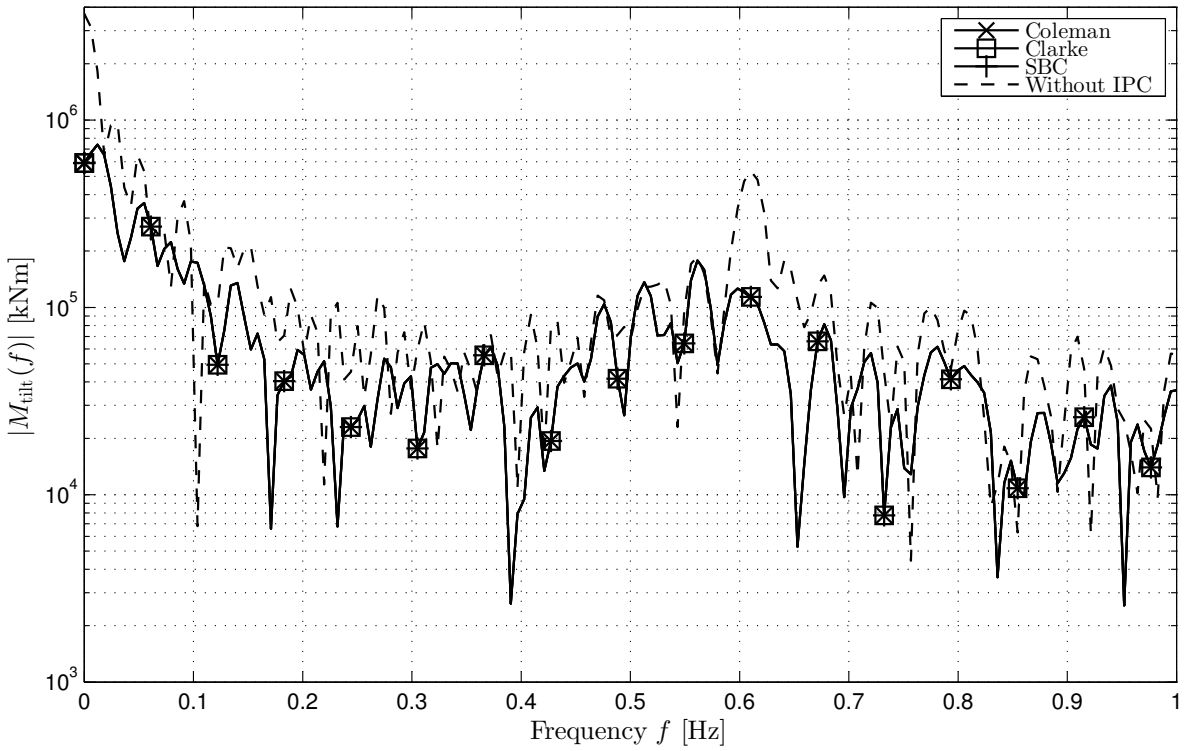

(b) Power spectrum of the main bearing tilt bending moment with fixed rotor speed.

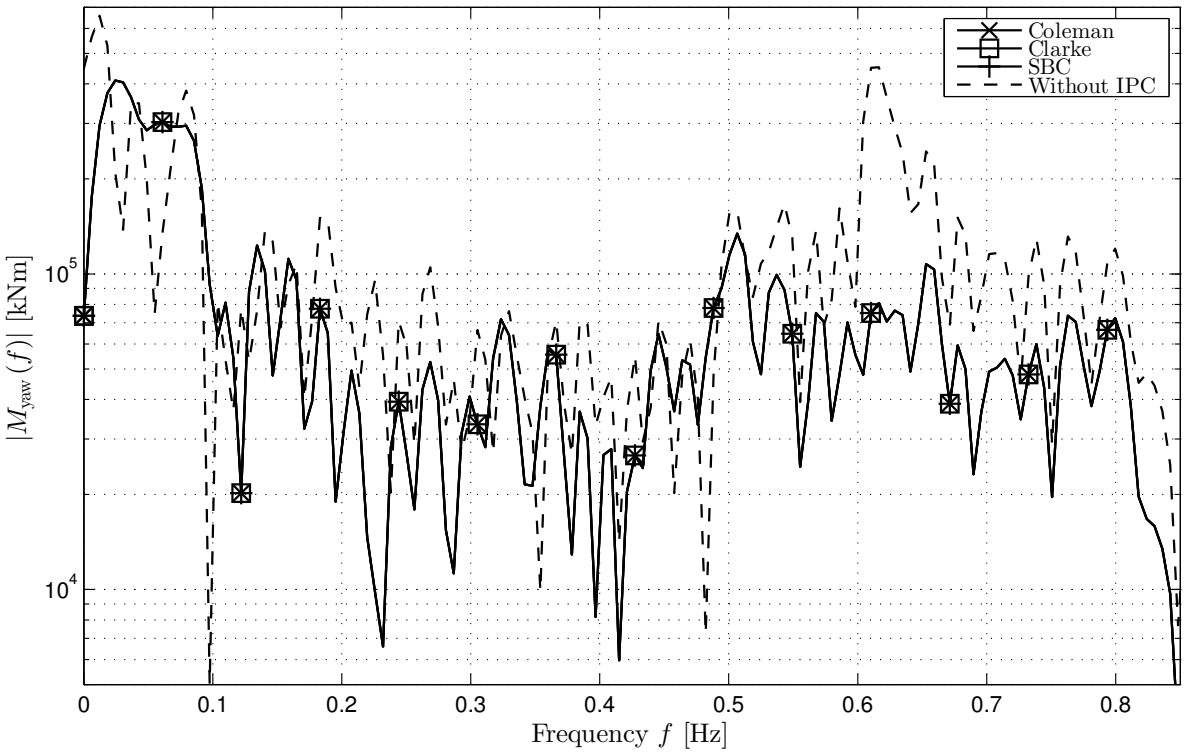

(c) Power spectrum of the main bearing yaw bending moment with fixed rotor speed.

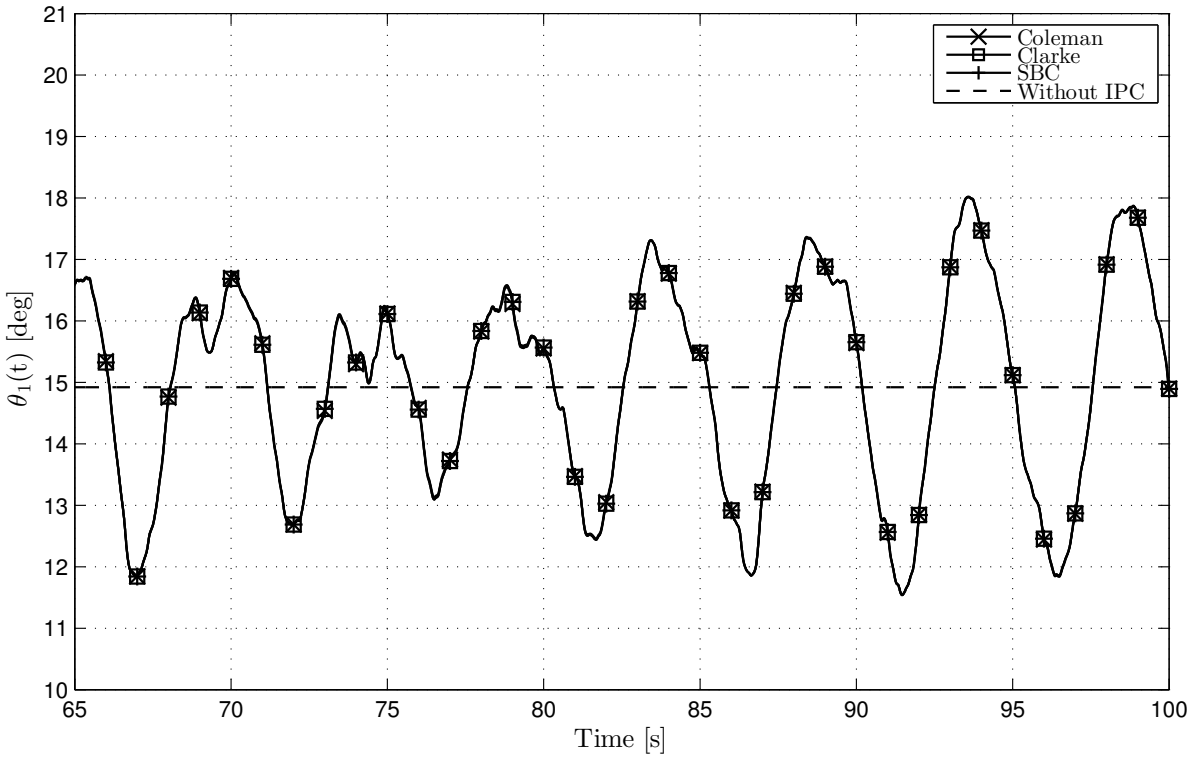

(d) Time history of the blade-pitch angle of blade 1 with fixed rotor speed. Similar results are obtained for the remaining blades.

Figure 7. Simulation results upon the NREL 5MW turbine with fixed rotor speed, showing indistinguishable performance between the various IPCs studied in this paper.

amounting to the installation of three identical SISO control systems. On the other hand, the implementation of Coleman and Clarke Transform-based controllers is slightly more involved, with both being MIMO and the Coleman controller in particular requiring a measurement of the rotor azimuth angle. However, if load reductions on the fixed turbine structure are a priority, then the natural environment in which to design such a controller is in the tilt and yaw frame of reference, motivating the design of a structured Coleman Transform-based controller. Of course, this could then be referred back to the rotating frame of reference for implementation as either a single-blade or Clarke Transform-based controller, via the relationships established in Lemmas 1 and 2.

5. Conclusions and Future Work

This paper established the links between three different IPC techniques; those based on the Clarke and Coleman Transforms and single-blade control. The equivalence between single-blade and a structured Coleman Transform-based controller was established, as was the equivalence between the latter and Clarke-Transform-based control. Under an assumption of fixed rotor speed, analytical and numerical results were presented that showed no performance difference between these IPCs, as quantified by the robust stability margin (2). Choice of IPC thus largely rests with preference of design and implementation.

Future work will look to accommodate the influence of tower motion in the design of IPCs, with a view towards removing the need for measurements of tower fore-aft motion. It is surmised that particular IPC architectures may lend themselves more readily to achieving this, and so may yet influence the issue of 'best' choice of IPC.

Appendix A. Proof of Theorem 1.

The proof is based on the derivation and comparison of the $\mathcal{H}_\infty$-norms of the shaped systems $H(PC_{\rm sbc}, I)$, $H(PC_{\rm ck}, I)$ and $H(PC_{\rm cm}, I)$. Proceeding with the former we obtain:

$$\|H(PC_{\rm sbc}, I)\|_\infty := \left\| \begin{bmatrix} C_{\rm sbc}P \\ I \end{bmatrix} (I - C_{\rm sbc}P)^{-1} \begin{bmatrix} -I & I \end{bmatrix} \right\|_\infty = \left\| \begin{bmatrix} T & 0 & 0 & -T & 0 & 0 \\ 0 & T & 0 & 0 & -T & 0 \\ 0 & 0 & T & 0 & 0 & -T \\ S & 0 & 0 & -S & 0 & 0 \\ 0 & S & 0 & 0 & -S & 0 \\ 0 & 0 & S & 0 & 0 & -S \end{bmatrix} \right\|_\infty ,$$

where $S(j\omega) := 1/(GK-1)(j\omega)$ and $T := GK/(GK-1)(j\omega)$ denote the sensitivity and complementary sensitivity functions, respectively. We are concerned with the spectrum of the following operator:

$$H(PC_{\rm sbc}, I)^* H(PC_{\rm sbc}, I) = \begin{bmatrix} X_{11} & X_{12} \\ X_{21} & X_{22} \end{bmatrix}, \tag{A1}$$

where:

$$X_{11} = -X_{12} = -X_{21} = X_{22} = \begin{bmatrix} S^*S + T^*T & 0 & 0 \\ 0 & S^*S + T^*T & 0 \\ 0 & 0 & S^*S + T^*T \end{bmatrix}$$

Next, noting that all four sub-matrices commute, the characteristic polynomial of (A1) can be expressed as follows (Silvester, 2000):

$$\det\left(\lambda I - H(PC_{\text{sbc}}, I)^* H(PC_{\text{sbc}}, I)\right) = (\lambda I - X_{11})(\lambda I - X_{22}) - X_{12}X_{21} = \lambda^3(\lambda - 2(S^*S + T^*T))^3.$$

The $\mathcal{H}_\infty$ norm of $H(PC_{\text{sbc}}, I)$ is therefore:

$$\|H(PC_{\text{sbc}}, I)\|_\infty = \sup_\omega \sqrt{2\left(S^*S + T^*T\right)} = \|H(GK, 1)\|_\infty . \tag{A2}$$

Turning attention to $H(PC_{\text{ck}}, I)$, we begin by taking the singular value decomposition of C_{ck}:

$$C_{\text{ck}}(j\omega) = \underbrace{\begin{bmatrix} -\sqrt{2/3} & 0 & 1/\sqrt{3} \\ 1/\sqrt{6} & -1/\sqrt{2} & 1/\sqrt{3} \\ 1/\sqrt{6} & 1/\sqrt{2} & 1/\sqrt{3} \end{bmatrix}}_{U_{\text{ck}}} \underbrace{\begin{bmatrix} K(j\omega) & 0 & 0 \\ 0 & K(j\omega) & 0 \\ 0 & 0 & 0 \end{bmatrix}}_{\tilde{C}_{\text{ck}}(j\omega)} \underbrace{\begin{bmatrix} -\sqrt{2/3} & 1/\sqrt{6} & 1/\sqrt{6} \\ 0 & -1/\sqrt{2} & 1/\sqrt{2} \\ -1/\sqrt{6} & -1/\sqrt{6} & -1/\sqrt{6} \end{bmatrix}}_{V_{\text{ck}}^*}$$

Inserting this into $\|H(PC_{\text{ck}}, I)\|_\infty$ yields:

$$\begin{aligned} \|H(PC_{\text{ck}}, I)\|_\infty &:= \left\| \begin{bmatrix} C_{\text{ck}}P \\ I \end{bmatrix} (I - C_{\text{ck}}P)^{-1} \begin{bmatrix} -I & I \end{bmatrix} \right\|_\infty , \\ &= \left\| \begin{bmatrix} \tilde{C}_{\text{ck}}P \\ U_{\text{ck}}^* V_{\text{ck}} \end{bmatrix} (U_{\text{ck}}^* V_{\text{ck}} - \tilde{C}_{\text{ck}}P)^{-1} \begin{bmatrix} -U_{\text{ck}}^* V_{\text{ck}} & U_{\text{ck}}^* V_{\text{ck}} \end{bmatrix} \right\|_\infty , \\ &= \left\| \tilde{H}(PC_{\text{ck}}, I) \right\|_\infty , \end{aligned}$$

where:

$$\tilde{H}(PC_{\text{ck}}, I) := \begin{bmatrix} -T & 0 & 0 & -T & 0 & 0 \\ 0 & -T & 0 & 0 & -T & 0 \\ 0 & 0 & 0 & 0 & 0 & 0 \\ -S & 0 & 0 & -S & 0 & 0 \\ 0 & -S & 0 & 0 & -S & 0 \\ 0 & 0 & -1 & 0 & 0 & -1 \end{bmatrix}.$$

It can be shown that the characteristic polynomial of $\tilde{H}(PC_{\text{ck}}, I)^* \tilde{H}(PC_{\text{ck}}, I)$ is given by:

$$\det(\lambda I - \tilde{H}(PC_{\text{ck}}, I)^* \tilde{H}(PC_{\text{ck}}, I)) = \lambda^3(\lambda - 2)(\lambda - 2(S^*S + T^*T))^2.$$

The relative degree of G ensures $\sup_\omega(S^*S + T^*T) \geq 1$, hence:

$$\|H(PC_{\text{ck}}, I)\|_\infty = \sup_\omega \sqrt{2\left(S^*S + T^*T\right)}. \tag{A3}$$

With respect to $H(P_{\text{cm}}C_{\text{cm}}, I)$, the singular value decomposition of P_{cm} is as follows:

$$P_{\text{cm}}(j\omega, \omega_0) = \underbrace{\begin{bmatrix} \frac{j}{\sqrt{2}} & \frac{-j}{\sqrt{2}} \\ \frac{1}{\sqrt{2}} & \frac{1}{\sqrt{2}} \end{bmatrix}}_{U_{\text{cm}}} \underbrace{\begin{bmatrix} G(j(\omega - \omega_0)) & 0 \\ 0 & G(j(\omega + \omega_0)) \end{bmatrix}}_{\tilde{P}_{\text{cm}}(j\omega, \omega_0)} \underbrace{\begin{bmatrix} \frac{-j}{\sqrt{2}} & \frac{1}{\sqrt{2}} \\ \frac{j}{\sqrt{2}} & \frac{1}{\sqrt{2}} \end{bmatrix}}_{U_{\text{cm}}^*}$$

Similarly, $C_{\rm cm} = U_{\rm cm}\tilde{C}_{\rm cm}U^*_{\rm cm}$, where:

$$\tilde{C}_{\rm cm}(j\omega,\omega_0) := \begin{bmatrix} K(j(\omega-\omega_0)) & 0 \\ 0 & K(j(\omega+\omega_0)) \end{bmatrix}$$

Inserting these into $\|H(P_{\rm cm}C_{\rm cm},I)\|_\infty$ yields:

$$\begin{aligned}\|H(PC_{\rm cm},I)\|_\infty &:= \left\| \begin{bmatrix} C_{\rm cm}P_{\rm cm} \\ I \end{bmatrix} (I - C_{\rm cm}P_{\rm cm})^{-1} \begin{bmatrix} -I & I \end{bmatrix} \right\|_\infty, \\ &= \left\| \begin{bmatrix} \tilde{C}_{\rm cm}\tilde{P}_{\rm cm} \\ I \end{bmatrix} (I - \tilde{C}_{\rm cm}\tilde{P}_{\rm cm})^{-1} \begin{bmatrix} -I & I \end{bmatrix} \right\|_\infty, \\ &= \left\| \tilde{H}(PC_{\rm cm},I) \right\|_\infty,\end{aligned}$$

in which:

$$\tilde{H}(PC_{\rm cm},I) := \begin{bmatrix} T_- & 0 & -T_- & 0 \\ 0 & T_+ & 0 & -T_+ \\ S_- & 0 & -S_- & 0 \\ 0 & S_+ & 0 & -S_+ \end{bmatrix},$$

where $S_-(j\omega,\omega_0) := 1/(GK-1)(j(\omega-\omega_0))$ and $S_+(j\omega,\omega_0) := 1/(GK-1)(j(\omega+\omega_0))$ are the frequency shifted sensitivity functions, and $T_-(j\omega,\omega_0) := GK/(GK-1)(j(\omega-\omega_0))$ and $T_+(j\omega,\omega_0) := GK/(GK-1)(j(\omega+\omega_0))$ are the shifted complimentary sensitivity functions. It can be shown that the characteristic polynomial of $\tilde{H}(P_{\rm cm}C_{\rm cm},I)^*\tilde{H}(P_{\rm cm}C_{\rm cm},I)$ is given by:

$$\det(\lambda I - \tilde{H}(P_{\rm cm}C_{\rm cm},I)^*\tilde{H}(P_{\rm cm}C_{\rm cm},I)) = \lambda^2(\lambda - 2(S_-^*S_- + T_-^*T_-))(\lambda - 2(S_+^*S_+ + T_+^*T_+)).$$

The $\mathcal{H}_\infty$ norm of $H(P_{\rm cm}C_{\rm cm},I)$ is thus given by:

$$\|H(P_{\rm cm}C_{\rm cm},I)\|_\infty = \sup_\omega \sqrt{2\left(S_-^*S_- + T_-^*T_-\right)} = \sup_\omega \sqrt{2\left(S_+^*S_+ + T_+^*T_+\right)} = \sup_\omega \sqrt{2\left(S^*S + T^*T\right)}. \tag{A4}$$

Appendix B. Transfer function of the blade controller K

The transfer function K of the $\mathcal{H}_\infty$ loop-shaping controller synthesised from (14) is as follows:

$$K(s) = \frac{N(s)}{D(s)}, \tag{B1}$$

where

$$\begin{aligned} N(s) &= 1.03\times10^{-6}s^9 + 5.55\times10^{-6}s^8 + 4.93\times10^{-5}s^7 + 1.74\times10^{-4}s^6 + 6.40\times10^{-4}s^5 \\ &\quad + 1.24\times10^{-3}s^4 + 9.00\times10^{-4}s^3 + 2.17\times10^{-3}s^2 - 1.38\times10^{-3}s + 9.84\times10^{-5} \\ D(s) &= s^9 + 9.40s^8 + 87.22s^7 + 353.20s^6 + 1955.00s^5 + 3031.00s^4 \\ &\quad + 1.12\times10^4s^3 + 7662.00s^2 + 1.33\times10^4s + 5663.00 \end{aligned}$$

References

Barlas, T., & van Kuik, G. (2010, January). Review of state of the art in smart rotor control research for wind turbines. *Progress in Aerospace Sciences*, *46*(1), 1–27. Retrieved from http://linkinghub.elsevier.com/retrieve/pii/S0376042109000293 doi:

Bossanyi, E. (2003, April). Individual Blade Pitch Control for Load Reduction. *Wind Energy*, *6*(2), 119–128. Retrieved from http://doi.wiley.com/10.1002/we.76 doi:

Bossanyi, E. (2005). Further load reductions with individual pitch control. *Wind Energy*, *8*(4), 481–485. Retrieved from http://onlinelibrary.wiley.com/doi/10.1002/we.166/abstract

Bossanyi, E., & Wright, A. (2009). Field testing of individual pitch control on the nrel cart-2 wind turbine. In *Ewec2009-european wind energy conference & exhibition.*

Coleman, R. P., & Feingold, A. M. (1957). Theory of self-excited mechanical oscillations of helicopter rotors with hinged blades. *National Advisory Committee for Aeronautics*.

Engels, W., Subhani, S., Zafar, H., & Savenije, F. (2014). Extending wind turbine operational conditions; a comparison of set point adaptation and lqg individual pitch control for highly turbulent wind. In *Journal of physics: Conference series* (Vol. 524, p. 012058).

Geyler, M., & Caselitz, P. (2008). Robust multivariable pitch control design for load reduction on large wind turbines. *Journal of solar energy engineering*, *130*(3), 030301–1. Retrieved from http://cat.inist.fr/?aModele=afficheN&cpsidt=20604937

Han, Y., & Leithead, W. (2014). Combined wind turbine fatigue and ultimate load reduction by individual blade control. In *Journal of physics: Conference series* (Vol. 524, p. 012062).

Jonkman, B. J. (2009). *TurbSim User's Guide: Version1.50* (Tech. Rep.). National Renewable Energy Laboratory.

Jonkman, J., & Buhl Jr, M. (2005). *FAST user's guide* (Tech. Rep.). National Renewable Energy Laboratory. Retrieved from https://wind.nrel.gov/designcodes/simulators/fast/FAST.pdf

Jonkman, J., Butterfield, S., Musial, W., & Scott, G. (2009). *Definition of a 5-MW Reference Wind Turbine for Offshore System Development* (Tech. Rep.). National Renewable Energy Laboratory.

Lackner, M. A., & van Kuik, G. (2010). A comparison of smart rotor control approaches using trailing edge flaps and individual pitch control. *Wind Energy*, *13*(2-3), 117–134.

Leithead, W., Neilson, V., & Dominguez, S. (2009). Alleviation of unbalanced rotor loads by single blade controllers. In *European wind energy conference (ewec 2009).* Retrieved from http://strathprints.strath.ac.uk/28424/

Leithead, W. E., Neilson, V., Dominguez, S., & Dutka, A. (2009). A novel approach to structural load control using intelligent actuators. In *Mediterranean conference on control & automation* (pp. 1257–1262). Retrieved from http://ieeexplore.ieee.org/xpls/abs_all.jsp?arnumber=5164719

Lu, Q., Bowyer, R., & Jones, B. (2014). Analysis and design of coleman transform-based individual pitch controllers for wind-turbine load reduction. *Wind Energy*, n/a–n/a. Retrieved from http://dx.doi.org/10.1002/we.1769 doi:

Muljadi, E., & Butterfield, C. P. (2001). Pitch-controlled variable-speed wind turbine generation. *Industry Applications, IEEE Transactions on*, *37*(1), 240–246. Retrieved from http://ieeexplore.ieee.org/xpls/abs_all.jsp?arnumber=903156

Pao, L., & Johnson, K. (2009). A tutorial on the dynamics and control of wind turbines and wind farms. *American Control Conference*. Retrieved from http://ieeexplore.ieee.org/xpls/abs_all.jsp?arnumber=5160195

Plumley, C., Leithead, W., Jamieson, P., Bossanyi, E., & Graham, M. (2014, June). Comparison of individual pitch and smart rotor control strategies for load reduction. *The Science of Making Torque from Wind 2014 (TORQUE 2014)*, *524*, 012054. Retrieved from http://stacks.iop.org/1742-6596/524/i=1/a=012054?key=crossref.aef1b20fff51552e3743076e267fb2d1 doi:

Selvam, K., Kanev, S., van Wingerden, J. W., van Engelen, T., & Verhaegen, M. (2009). Feedback–feedforward individual pitch control for wind turbine load reduction. *International Journal of Robust and Nonlinear Control*(April 2008), 72–91. Retrieved from http://onlinelibrary.wiley.com/doi/10.1002/rnc.1324/abstract doi:

Silvester, J. R. (2000). Determinants of block matrices. *The Mathematical Gazette*, *84*(501), 460-467. Retrieved from http://www.jstor.org/stable/3620776

Stol, K., Moll, H., Bir, G., & Namik, H. (2009). A comparison of multi-blade coordinate transformation and direct periodic techniques for wind turbine control design. In *47th aiaa/asme* (pp. 1–12). Retrieved

from http://arc.aiaa.org/doi/pdf/10.2514/6.2009-479

van Engelen, T. G. (2006). Design model and load reduction assessment for multi-rotational mode individual pitch control (higher harmonics control). In *European wind energy conference* (pp. 6–68).

van Engelen, T. G., & van der Hooft, E. L. (2005). *Individual Pitch Control Inventory* (Tech. Rep.). ECN.

Vas, P. (1992). *Electrical machines and drives: a space-vector theory approach*. Oxford University Press.

Vinnicombe, G. (2001). *Uncertainty and feedback*. Imperial College Press.

Zhang, Y., Chen, Z., & Cheng, M. (2013, May). Proportional resonant individual pitch control for mitigation of wind turbines loads. *IET Renewable Power Generation*, *7*(3), 191–200. Retrieved from http://digital-library.theiet.org/content/journals/10.1049/iet-rpg.2012.0282 doi: